

# Crystal Structure, Structural Disorder, and Hydration Behavior of Calcium Zirconium Aluminate, $\text{Ca}_7\text{ZrAl}_6\text{O}_{18}$

Koichiro Fukuda,\* Tomoyuki Iwata, and Kenjiro Nishiyuki

Department of Environmental and Materials Engineering, Nagoya Institute of Technology,  
Nagoya 466-8555, Japan

Received March 16, 2007. Revised Manuscript Received May 25, 2007

Crystal structure, structural disorder, and hydration behavior of  $\text{Ca}_7\text{ZrAl}_6\text{O}_{18}$  were investigated by laboratory X-ray powder diffraction ( $\text{Cu K}\alpha_1$ ) and conduction calorimetry. The initial structural model with 21 independent atoms in the unit cell was determined using direct methods, and it was further modified to a split-atom model, in which the five types of Ca atoms and four types of  $\text{AlO}_4$  tetrahedra were, respectively, positionally and orientationally disordered. The crystal structure is orthorhombic (space group  $Pmn2_1$ ,  $Z = 2$ ) with lattice dimensions  $a = 1.08486(1)$  nm,  $b = 1.05913(1)$  nm,  $c = 0.766945(8)$  nm, and  $V = 0.88123(1)$  nm<sup>3</sup>. The electron density distribution was determined by the maximum-entropy methods-based pattern fitting method, which resulted in the final reliability indices of  $R_{\text{wp}} = 9.59\%$  ( $S = 1.22$ ),  $R_p = 7.16\%$ ,  $R_B = 2.38\%$ , and  $R_F = 1.87\%$ . This compound showed the hydration behavior comparable to  $\text{Ca}_3\text{Al}_2\text{O}_6$ . The reaction of  $\text{Ca}_7\text{ZrAl}_6\text{O}_{18}$  with water gave hydrogarnet as the main crystalline product. Addition of gypsum effectively retarded the hydration reaction, with the major hydration products of calcium monosulfo-aluminate hydrate and calcium aluminate hydrate.

## Introduction

In the system  $\text{CaO}-\text{ZrO}_2-\text{Al}_2\text{O}_3$  a new compound  $\text{Ca}_7\text{ZrAl}_6\text{O}_{18}$  has been found by Berezhnoi and Kordyuk<sup>1</sup> with the following properties: density 3.10 Mg/m<sup>3</sup>, melting point 1823 K, crystal biaxial, and interaction with water. To our knowledge, this is the only substance containing  $\text{ZrO}_2$  which has hydration reactivity.<sup>1,2</sup> Although its X-ray powder diffraction (XRPD) pattern is available, the crystal structure is still not elucidated so far.

Recent advances in the field of crystal-structure analysis from XRPD data have enabled us to investigate complex structures, including positional disordering of atoms and orientational disordering of atomic groups. To begin with initial structural models is required, which may be determined by, for example, direct methods.<sup>3</sup> The structural parameters are subsequently refined using the Rietveld method.<sup>4</sup> To disclose the structural details that had not been introduced into the structural models, the combined use of a maximum-entropy method (MEM)<sup>5</sup> and a MEM-based pattern fitting (MPF) method<sup>6</sup> is employed. The Rietveld and MEM analyses are insufficient to readily determine charge densities because the observed structure factors,  $F_o(\text{Rietveld})$ , are

biased toward the structural models. The subsequent MPF method reduces the bias as much as possible. Thus, the MEM and MPF analyses are alternately repeated (REMEDY cycle) until the reliability indices no longer decrease. Crystal structures are represented not by structural parameters but by electron densities in MPF.

$\text{Ca}_3\text{Al}_2\text{O}_6$  is highly reactive with water. The hydration products can be composed of both crystalline and amorphous materials. The crystalline products are two calcium aluminate hydrates of  $2\text{CaO}\cdot\text{Al}_2\text{O}_3\cdot 8\text{H}_2\text{O}$  ( $\text{C}_2\text{AH}_8$ ) and  $4\text{CaO}\cdot\text{Al}_2\text{O}_3\cdot 19\text{H}_2\text{O}$  ( $\text{C}_4\text{AH}_{19}$ ) immediately after contact with water at ordinary temperatures, and they gradually convert into hydrogarnet ( $\text{C}_3\text{AH}_6$ ).<sup>7</sup> Addition of gypsum ( $\text{CaSO}_4\cdot 2\text{H}_2\text{O}$ :  $\text{C}\bar{\text{S}}\text{H}_2$ ) substantially retards the hydration reaction and prevents premature setting, with the main hydration products of calcium monosulfo-aluminate hydrate ( $\text{C}_4\text{A}\bar{\text{S}}\text{H}_{12}$ ), calcium aluminate hydrate ( $\text{C}_4\text{AH}_{13}$ ), and ettringite ( $\text{C}_6\text{A}\bar{\text{S}}_3\text{H}_{32}$ ).<sup>7</sup> Each of these products is formed to an extent that depends on the ratio of gypsum to  $\text{Ca}_3\text{Al}_2\text{O}_6$ .

In the present study, we determined the initial structural model of  $\text{Ca}_7\text{ZrAl}_6\text{O}_{18}$  from XRPD data using direct methods and modified it into a split-atom model, in which the calcium atoms and  $\text{AlO}_4$  tetrahedra were, respectively, positionally and orientationally disordered. The compound was further characterized by the high hydration reactivity, which was comparable to that of  $\text{Ca}_3\text{Al}_2\text{O}_6$ .

## Experimental Section

**(1) Synthesis.** A specimen of  $\text{Ca}_7\text{ZrAl}_6\text{O}_{18}$  was prepared from stoichiometric amounts of reagent-grade chemicals  $\text{CaCO}_3$ ,  $\text{ZrO}_2$ ,

\* Corresponding author. E-mail: fukuda.koichiro@nitech.ac.jp.

- (1) Berezhnoi, A. S.; Kordyuk, R. A. *Dopov. Akad. Nauk Ukr. RSR* **1963**, 10, 1344–1347.
- (2) Berezhnoi, A. S.; Tarnopol'skaya, R. A. *Neorg. Mater. Akad. Nauk* **1968**, 4, 2151–2154.
- (3) Altomare, A.; Burla, M. C.; Camalli, M.; Carrozzini, B.; Cascarano, G. L.; Giacovazzo, C.; Guagliardi, A.; Moliterni, A. G. G.; Polidori, G.; Rizzi, R. *J. Appl. Crystallogr.* **1999**, 32, 339–340.
- (4) Rietveld, H. M. *J. Appl. Crystallogr.* **1969**, 2, 65–71.
- (5) Takata, M.; Nishibori, E.; Sakata, M. *Z. Kristallogr.* **2001**, 216, 71–86.
- (6) Izumi, F.; Kumazawa, S.; Ikeda, T.; Hu, W.-Z.; Yamamoto, A.; Oikawa, K. *Mater. Sci. Forum* **2001**, 378–381, 59–64.

- (7) Taylor, H. F. W. *Cement Chemistry*; Thomas Telford Publishing: London, U.K., 1997; pp 1–28.

and  $\text{Al}_2\text{O}_3$ . Well-mixed chemicals were pressed into pellets (12 mm diameter and 3 mm thick) and heated at 1673 K for 80 h, followed by quenching in air. The reaction product was a densely sintered polycrystalline material. It was finely ground using a micromill (P-7, Fritsch, Idar-oberstein, Germany) and sieved to obtain a fine powder specimen with particle sizes less than 44  $\mu\text{m}$ .

**(2) X-ray Powder Diffraction.** XRPD intensities were collected at 298 K on a PANalytical X'Pert PRO Alpha-1 diffractometer equipped with a high-speed detector (X'Celerator) in the Bragg–Brentano geometry in a  $2\theta$  range from  $10.0012^\circ$  to  $148.4958^\circ$  using monochromatized  $\text{Cu K}\alpha_1$  radiation (45 kV, 40 mA). The divergence slit of  $0.25^\circ$  was employed to collect the quantitative profile intensities over the whole  $2\theta$  range. Other experimental conditions were as follows: continuous scan, total of 16 576 data points, and total experimental time of 29.5 h. The positional parameters of atoms were standardized using the computer program STRUCTURE TIDY.<sup>8</sup> The three-dimensional EDD and crystal-structure models were visualized using the software package VENUS.<sup>9</sup>

**(3) Hydration.** The specific surface area of the powder specimen was measured by a BET (Brunauer–Emmet–Teller) method (FlowSorb III 2310, Shimadzu Co., Japan). The hydration behavior of pure  $\text{Ca}_7\text{ZrAl}_6\text{O}_{18}$  and  $\text{Ca}_7\text{ZrAl}_6\text{O}_{18}$  together with reagent gypsum ( $\text{Ca}_7\text{ZrAl}_6\text{O}_{18}/\text{gypsum} = 5.7$  by weight) was investigated in an isothermal heat flow calorimeter (TCC-23, Tokyo Rikou Co., Japan). Each powder specimen (10.0 g) was hydrated with a water/solid ratio of 1.0 by weight. The cumulative heat evolution at 293 K was measured for 7 d. The accuracy was estimated to be within 3 J/g from the calibration made by electric heating. The phase composition of the crystalline hydration products was determined from the XRPD patterns in a  $2\theta$  range from  $5.0^\circ$  to  $70.0^\circ$ .

## Results and Discussion

**(1) Initial Structural Model.** Peak positions of the experimental diffraction pattern were first determined using the computer program PowderX.<sup>10</sup> The  $2\theta$  values of 39 observed peak positions were then used as input data to the automatic indexing computer program TREOR90.<sup>11</sup> One orthorhombic unit cell was found with satisfactory figures of merit  $M_{20}/F_{20} = 17/19$  (0.009230, 118) and  $M_{39}/F_{39} = 13/15$  (0.006982, 385).<sup>12,13</sup> The derived unit-cell parameters of  $a = 1.08549$  nm,  $b = 1.06012$  nm, and  $c = 0.76738$  nm could index all the observed reflections in the experimental diffraction pattern.

The integrated intensities were refined by the whole powder-pattern decomposition method, based on the Pawley algorithm,<sup>14</sup> using the computer program WPPF.<sup>15</sup> The observed diffraction peaks were examined to determine the presence or absence of reflections. Systematic absences  $h + l \neq 2n$  for  $h0l$ ,  $h \neq 2n$  for  $h00$ , and  $l \neq 2n$  for  $00l$  reflections were found, which implied that possible space groups were  $Pmn2_1$ ,  $P2_1nm$ , and  $Pmnm$ . All of the possible space groups were tested using the EXPO2004 package<sup>3</sup> for the search of a crystal-structure model. A promising structural

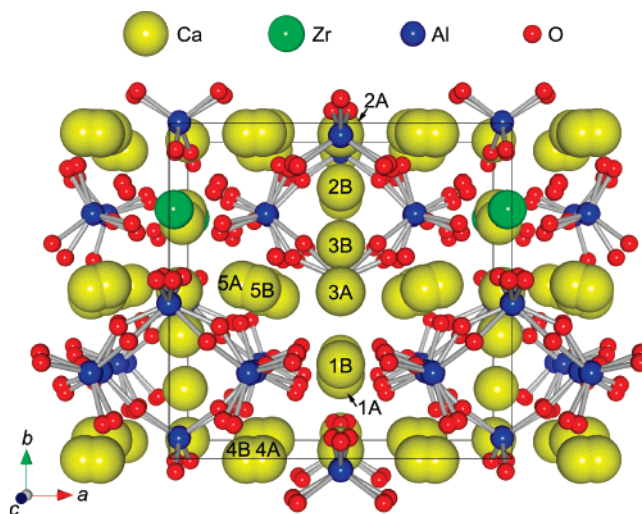


**Figure 1.** Perspective  $c$ -axis projection of  $\text{Ca}_7\text{ZrAl}_6\text{O}_{18}$ . Numbering of Ca atoms corresponds to that given in Table 2.

**Table 1. Crystal Data for  $\text{Ca}_7\text{ZrAl}_6\text{O}_{18}$**

chemical composition	$\text{Ca}_7\text{ZrAl}_6\text{O}_{18}$
space group	$Pmn2_1$
$a$ , nm	1.08486(1)
$b$ , nm	1.05913(1)
$c$ , nm	0.766945(8)
$V$ , nm <sup>3</sup>	0.88123(1)
$Z$	2
$D_x$ , Mg m <sup>-3</sup>	3.10

**Table 2. Atomic Coordinates and Isotropic Displacement Parameters for  $\text{Ca}_7\text{ZrAl}_6\text{O}_{18}$**

site	Wyckoff position	$g$	$x$	$y$	$z$	$100 \times B$ , nm <sup>2</sup>
Ca1A	2a	0.56(2)	0	0.759(1)	0.218(2)	0.9(1)
Ca1B	2a	0.44	0	0.723(1)	0.326(2)	0.9
Ca2A	2a	0.62(1)	0	0.004(1)	0.018(2)	1.4(2)
Ca2B	2a	0.38	0	0.179(1)	0.170(2)	1.4
Ca3A	2a	0.68(1)	0	0.502(1)	0.486(2)	1.2(1)
Ca3B	2a	0.32	0	0.359(1)	0.365(2)	1.2
Ca4A	4b	0.39(3)	0.234(1)	0.015(1)	0.286(2)	0.7(1)
Ca4B	4b	0.61	0.282(2)	0.0171(9)	0.284(2)	0.7
Ca5A	4b	0.29(2)	0.297(2)	0.481(1)	0.224(3)	0.5(1)
Ca5B	4b	0.71	0.252(1)	0.4924(7)	0.241(2)	0.5
Zr	2a	1	0	0.7511(4)	0.755(1)	1.14(3)
Al1	2a	1	0	0.462(1)	0	0.37(4)
Al2	2a	1	0	0.035(1)	0.4939(9)	0.37
Al3	4b	1	0.2689(9)	0.7454(6)	0.472(2)	0.37
Al4	4b	1	0.2374(9)	0.2468(7)	0.537(2)	0.37
O1	2a	1	0	0.939(1)	0.679(2)	1.4(1)
O2	4b	1	0.189(1)	0.397(1)	0.479(3)	1.4
O3	4b	1	0.2246(6)	0.7278(9)	0.255(2)	1.4
O4	4b	0.5	0.023(3)	0.532(1)	0.203(3)	0.7
O5	4b	0.5	0.476(3)	0.051(1)	0.803(3)	0.7
O6	4b	0.5	0.471(1)	0.456(1)	0.307(3)	0.7
O7A	4b	0.5	0.372(3)	0.201(4)	0.431(7)	0.7
O7B	4b	0.5	0.359(3)	0.175(3)	0.428(7)	0.7
O8A	4b	0.5	0.138(3)	0.121(3)	0.491(6)	0.7
O8B	4b	0.5	0.125(2)	0.130(2)	0.553(3)	0.7
O9A	4b	0.5	0.114(2)	0.350(1)	0.057(3)	0.7
O9B	4b	0.5	0.352(2)	0.606(2)	0.500(5)	0.7
O10A	4b	0.5	0.362(3)	0.289(3)	0.096(4)	0.7
O10B	4b	0.5	0.372(2)	0.316(3)	0.036(3)	0.7
O11A	4b	0.5	0.189(3)	0.103(3)	0.039(6)	0.7
O11B	4b	0.5	0.159(2)	0.114(2)	0.030(4)	0.7

model with a minimum reliability index  $R_F$ <sup>16</sup> of 15.5% was found with the space group  $Pmn2_1$  in a default run of the program. There were 21 independent atoms in the unit cell;

(8) Gelato, L. M.; Parthé, E. *J. Appl. Crystallogr.* **1987**, *20*, 139–143.

(9) Izumi, F.; Dilanian, R. A. *Commission on Powder Diffraction, IUCr Newsl.* **2005**, *32*, 59–63.

(10) Dong, C. *J. Appl. Crystallogr.* **1999**, *32*, 838.

(11) Werner, P. E.; Eriksson, L.; Westdahl, M. *J. Appl. Crystallogr.* **1985**, *18*, 367–370.

(12) de Wolff, P. M. *J. Appl. Crystallogr.* **1968**, *1*, 108–113.

(13) Smith, G. S.; Snyder, R. L. *J. Appl. Crystallogr.* **1979**, *12*, 60–65.

(14) Pawley, G. S. *J. Appl. Crystallogr.* **1981**, *14*, 357–361.

(15) Toraya, H. *J. Appl. Crystallogr.* **1986**, *19*, 440–447.

(16) Young, R. A. In *The Rietveld Method*; Young, R. A., Ed.; Oxford University Press: Oxford, U.K., 1993; pp 1–38.

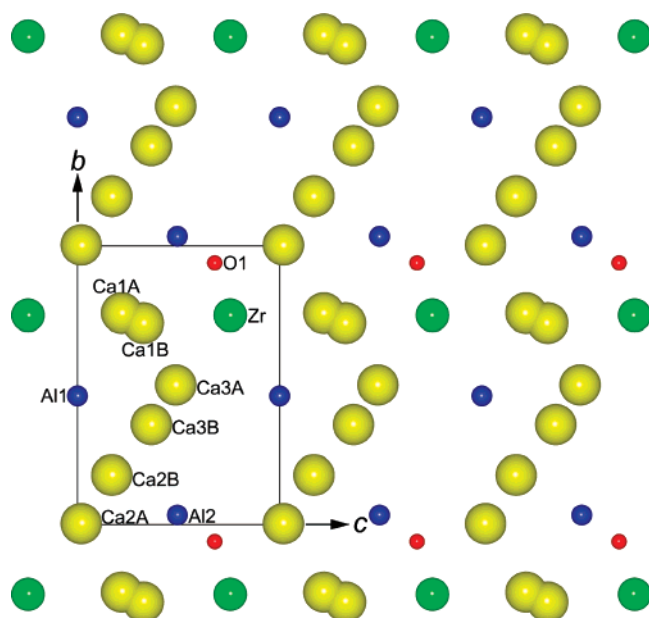


**Figure 2.** Atom arrangement of  $\text{Ca}_7\text{ZrAl}_6\text{O}_{18}$  on (100) at  $x = 0$ . Numbering of atoms corresponds to that given in Table 2. The Ca2A, Ca2B, Ca3B, Ca3A, and Zr atoms are oriented nearly on-line along [011].

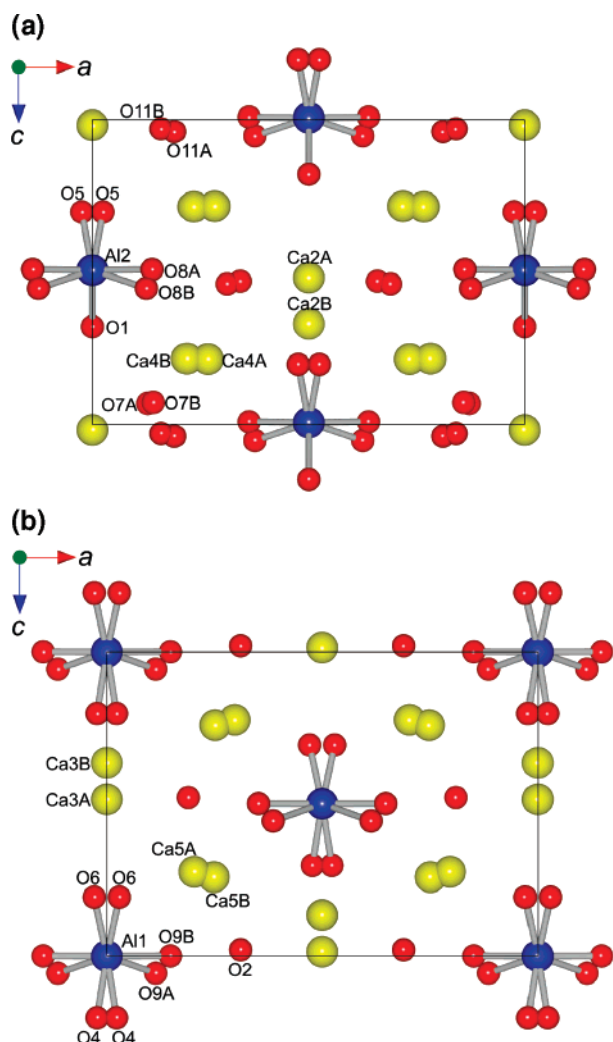


**Figure 3.** Projection of  $\text{Ca}_7\text{ZrAl}_6\text{O}_{18}$  onto (010) in the regions of (a)  $-0.21 \leq y \leq 0.17$  and (b)  $0.35 \leq y \leq 0.65$ .

one Zr atom, three Ca atoms (Ca1, Ca2, and Ca3), two Al atoms (Al1 and Al2), and four O atoms (O1, O4, O5, and

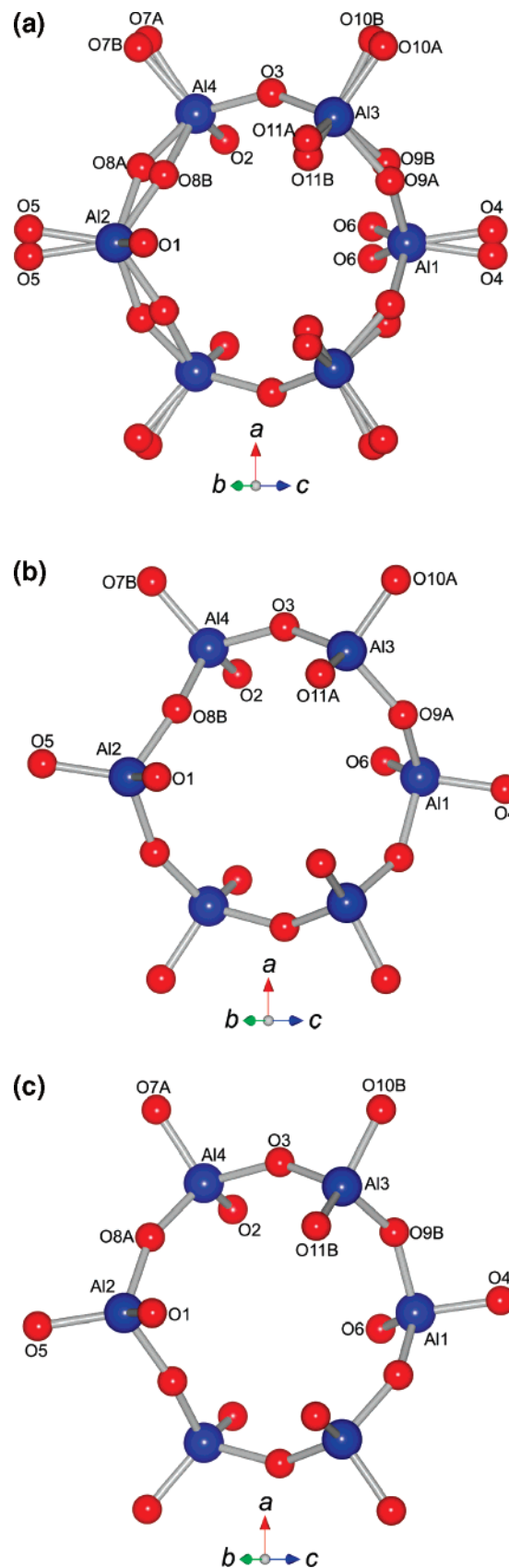


**Figure 4.** Projection of (a) disordered  $\text{Al}_6\text{O}_{18}$  ring and (b and c) ordered  $\text{Al}_6\text{O}_{18}$  rings viewed along [011]. The two structural configurations in parts b and c are related by the pseudo-symmetry (100) mirror plane passing through the Al1, Al2, and O1 atoms.

O6) were located on the special position (Wyckoff position  $2a$ ), and the rest of the atoms (Ca4, Ca5, Al3, Al4, O2, O3,



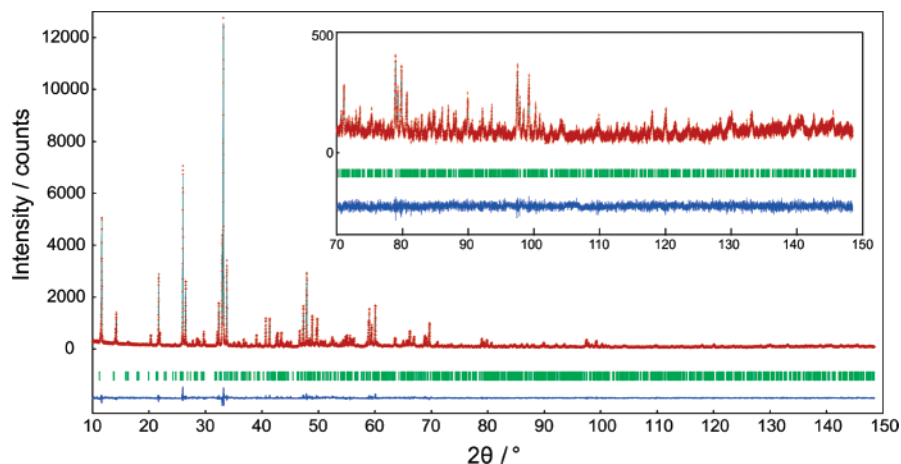


**Figure 5.** Comparison of the observed diffraction pattern of  $\text{Ca}_7\text{ZrAl}_6\text{O}_{18}$  (symbol: +) with the corresponding calculated pattern (upper solid line). The difference curve is shown in the lower part of the diagram. Vertical bars indicate the positions of Bragg reflections.

**Table 3.** Al–O Bond Lengths (nm) and O–Al–O Angles (deg) in  $\text{Ca}_7\text{ZrAl}_6\text{O}_{18}$

Al1–O4	0.174(2)	Al2–O1	0.174(2)	Al3–O11A	0.174(4)	Al4–O2	0.174(1)
Al1–O6	0.174(2)	Al2–O5	0.174(2)	Al3–O3	0.174(1)	Al4–O7B	0.174(3)
Al1–O9B	0.176(3)	Al2–O8B	0.175(2)	Al3–O10A	0.174(3)	Al4–O8B	0.174(2)
Al1–O9A	0.176(2)	Al2–O8A	0.176(3)	Al3–O9A	0.175(2)	Al4–O3	0.174(2)
$\langle \text{Al1–O} \rangle$	0.175	$\langle \text{Al2–O} \rangle$	0.175	$\langle \text{Al3–O} \rangle$	0.174	$\langle \text{Al4–O} \rangle$	0.174
O4–Al1–O9B	92.6(18)	O1–Al2–O8B	97.0(12)	O11A–Al3–O9A	103.5(16)	O2–Al4–O3	100.0(9)
O4–Al1–O9A	99.3(14)	O1–Al2–O8A	108.1(13)	O11A–Al3–O10A	104.0(19)	O8B–Al4–O3	102.0(9)
O6–Al1–O9B	111.4(15)	O8B–Al2–O8A	111.5(12)	O10A–Al3–O9A	105.6(17)	O7B–Al4–O8B	104.7(12)
O9B–Al1–O9A	111.4(13)	O1–Al2–O5	112.5(10)	O3–Al3–O10A	105.9(11)	O7B–Al4–O3	110.6(18)
O6–Al1–O9A	114.5(10)	O5–Al2–O8A	113.0(18)	O11A–Al3–O3	116.8(16)	O2–Al4–O8B	117.4(13)
O4–Al1–O6	125.3(11)	O5–Al2–O8B	113.6(12)	O3–Al3–O9A	119.5(9)	O2–Al4–O7B	120.4(20)
$\langle \text{O–Al1–O} \rangle$	109.1	$\langle \text{O–Al2–O} \rangle$	109.3	$\langle \text{O–Al3–O} \rangle$	109.2	$\langle \text{O–Al4–O} \rangle$	109.2

O7, O8, O9, O10, and O11) were located on the general position (4b). The prominent feature of the structural model is that six  $\text{AlO}_4$  tetrahedra are joined, sharing corners, to form an  $[\text{Al}_6\text{O}_{18}]$  rings.

Structural parameters were refined by the Rietveld method using the computer program RIETAN-FP.<sup>17</sup> A Legendre polynomial was fitted to background intensities with 12 adjustable parameters. The pseudo-Voigt function<sup>18</sup> was used to fit the experimental peak profiles. The isotropic displacement ( $B$ ) parameters of Al atoms were constrained to have the same value and those of the O atoms as well. The refinement resulted in the relatively large  $B$  parameters for the Ca and O sites ( $B(\text{Ca1}) = 2.3(2) \times 10^{-2} \text{ nm}^2$ ,  $B(\text{Ca2}) = 1.6(2) \times 10^{-2} \text{ nm}^2$ ,  $B(\text{Ca3}) = 12.8(6) \times 10^{-2} \text{ nm}^2$ ,  $B(\text{Ca4}) = 1.7(1) \times 10^{-2} \text{ nm}^2$ ,  $B(\text{Ca5}) = 1.7(1) \times 10^{-2} \text{ nm}^2$ , and  $B(\text{O}) = 2.3(1) \times 10^{-2} \text{ nm}^2$ ) with the less satisfactory reliability ( $R$ ) indices of  $R_{\text{wp}} = 16.30\%$  ( $S = R_{\text{wp}}/R_e = 2.08$ ),  $R_p = 12.52\%$ ,  $R_B = 10.57\%$ , and  $R_F = 3.66\%$ .<sup>16</sup> These findings prompted us to build split-atom models for Ca and O.

**(2) Split-Atom Model.** The splitting of atoms was performed in two different ways. One was to decrease the site symmetry from  $2a$  (point symmetry  $m$ ) to  $4b$  (1), and the other was to split each site into two fractions. When the Ca atoms on the  $2a$  sites (Ca1, Ca2, and Ca3) were shifted to those on the  $4b$  site, the  $R$  indices eventually increased. Thus we split every Ca site into two fractions to obtain the lower  $R$  indices of  $R_{\text{wp}} = 11.47\%$  ( $S = 1.46$ ),  $R_p = 8.78\%$ ,

$R_B = 4.93\%$ , and  $R_F = 2.69\%$ . The distribution of Ca atoms between each of the split sites, MA and MB ( $M = \text{Ca1, Ca2, Ca3, Ca4, and Ca5}$ ), was determined by imposing the following linear constraints on occupancies,  $g$ ,  $g(\text{MA}) + g(\text{MB}) = 1$ . The parameters  $B(\text{MA})$  and  $B(\text{MB})$  were constrained to be equal to each other. The common  $B$  parameter for all the O sites was still unusually large ( $= 2.33(7) \times 10^{-2} \text{ nm}^2$ ) because the split-atom model was imperfect.

In the subsequent Rietveld refinement, the O4, O5, and O6 sites were displaced from position  $2a$  to position  $4b$ , and each of the O7, O8, O9, O10, and O11 sites was split into two fractions. The  $B$  parameters of these sites, denoted by  $B(\text{Os})$ , were constrained to have the same value. Because splitting of the rest oxygen sites of O1, O2, and O3 yielded the  $R$  indices unchanged, they were kept unsplit for the final structural model. The following linear constraints were imposed on the  $B$  parameters:  $B(\text{O1}) = B(\text{O2}) = B(\text{O3}) = 2 \times B(\text{Os})$ . The final Rietveld refinement resulted in satisfactory  $B$  parameters for all the sites with  $R$  indices of  $R_{\text{wp}} = 9.66\%$ , ( $S = 1.23$ ),  $R_p = 7.20\%$ ,  $R_B = 3.59\%$ , and  $R_F = 2.27\%$ , indicating that highly disordered arrangements of Ca and O atoms can be represented adequately with the structural model. Crystal data are given in Table 1, and the final positional and  $B$  parameters of atoms are given in Table 2. The calculated density ( $D_x$ ) was in excellent agreement with that determined in a previous study.<sup>1</sup>

Figure 1 shows the perspective view of the crystal structure of  $\text{Ca}_7\text{ZrAl}_6\text{O}_{18}$ . Each of the Ca sites is split into two positions with a separation ranging from 0.053 to 0.218 nm; the individual distances are 0.091(1) nm for Ca1A–Ca1B, 0.218(2) nm for Ca2A–Ca2B, 0.177(2) nm for Ca3A–Ca3B,

(17) Izumi, F.; Ikeda, T. *Mater. Sci. Forum* **2000**, 321–324, 198–203.

(18) Toraya, H. *J. Appl. Crystallogr.* **1990**, 23, 485–491.

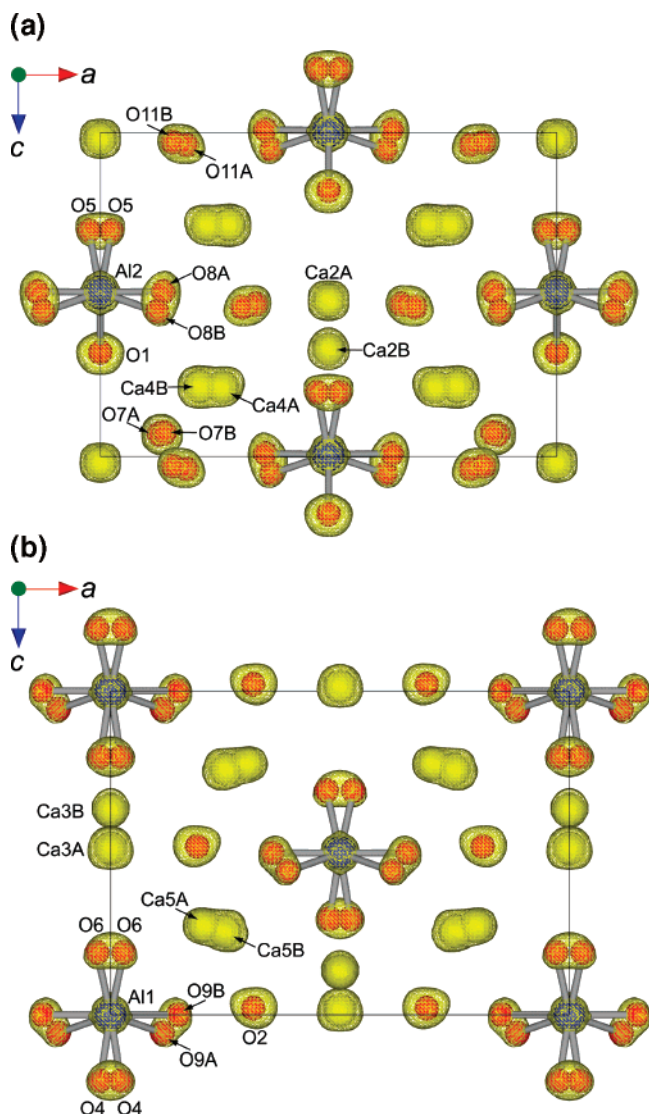


**Figure 6.** Electron density distribution determined by MPF in the regions of (a)  $-0.21 \leq y \leq 0.17$  and (b)  $0.35 \leq y \leq 0.65$ . Isosurfaces expressed in wireframe style for an equidensity level of  $0.003 \text{ nm}^{-3}$ .

0.053(1) nm for Ca4A–Ca4B, and 0.053(2) nm for Ca5A–Ca5B. The Ca1A, Ca1B, Ca2A, Ca2B, Ca3A, Ca3B, Zr, Al1, Al2, and O1 sites lie in (100) mirror planes at  $x = 0$  and  $x = 0.5$  (Figure 2). The five sites of Ca2A, Ca2B, Ca3B, Ca3A, and Zr are further oriented nearly on-line along<sup>011</sup> with  $x = 0$  and  $[01\bar{1}]$  with  $x = 0.5$ . Figure 3 illustrates part of the crystal structure in  $y$  ranges of  $-0.21 \leq y \leq 0.17$  and  $0.35 \leq y \leq 0.65$ , where the Ca2A, Ca2B, Al2, and O1 atoms are included in the former region, and the Ca3A, Ca3B, and Al1 atoms are included in the latter.

Because the Al1, Al2, and O1 atoms lie in (100) mirror planes, the disordered  $[\text{Al}_6\text{O}_{18}]$  ring (Figure 4a) can be regarded as a statistical average of the two mirror-related structural configurations. One of the two configurations is shown in Figure 4b, in which the bridging oxygen atoms of O3, O8B, and O9A are almost coplanar to one another, with the aluminum atoms alternately 8 nm up and down from the plane. The geometrical feature is exactly the same for the other  $[\text{Al}_6\text{O}_{18}]$  ring with different mirror-related orientations (Figure 4c). In Table 3, only Al–O bonds and O–Al–O angles belonging to one of the two mirror-related orientations

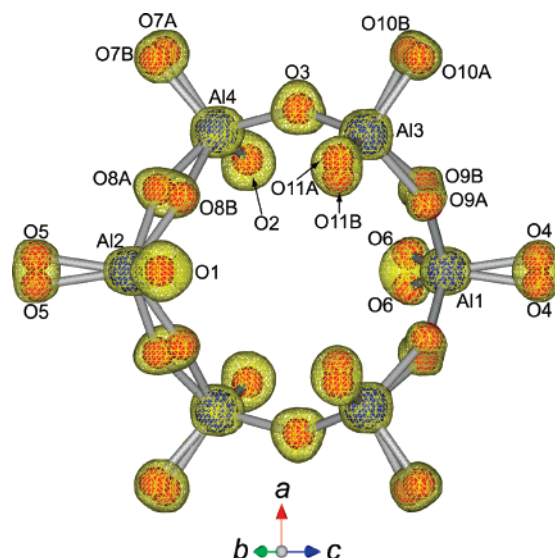


**Figure 7.** Electron density distribution determined by MPF with the disordered  $\text{Al}_6\text{O}_{18}$  ring. Isosurfaces expressed in wireframe style for an equidensity level of  $0.003 \text{ nm}^{-3}$ .

are reported, excluding the bonds and angles between atoms of different orientation states. The mean bond lengths and angles are in fair agreement with those of  $\text{Ca}_3\text{Al}_2\text{O}_6$  ( $\langle \text{Al}-\text{O} \rangle = 0.175 \text{ nm}$  and  $\langle \text{O}-\text{Al}-\text{O} \rangle = 109.4^\circ$ ).<sup>19</sup> The mean bond lengths are also in accord with the interatomic distance of 0.177 nm that is calculated from the ionic radii of  $\text{Al}^{3+}$  and  $\text{O}^{2-}$  in the fourfold coordination [ $r(\text{Al}^{3+}) = 0.039 \text{ nm}$  and  $r(\text{O}^{2-}) = 0.138 \text{ nm}$ ].<sup>20</sup>

**(3) Electron Density Distribution.** The MPF method was subsequently applied so as to extract structural details and consequently improve the EDD. After one REMEDY cycle,  $R_{\text{wp}}$  ( $S$ ),  $R_p$ ,  $R_B$ , and  $R_F$  decreased to 9.59% (1.22), 7.16%, 2.38%, and 1.87%, respectively. Subtle changes in EDD arose out of MPF, which improved the  $F_o(\text{MPF})$  data and consequently the  $R$  factors. The decreases in  $R$  indices demonstrate that the present disordered structure is better expressed with electron densities than with the structural parameters in Table 2. Observed, calculated, and difference XRPD patterns for the final MPF are plotted in Figure 5.

We expected MPF to disclose the structural details that had not been introduced into the above split-atom model. However, the EDD determined by MPF is explained sufficiently by the present split-atom model. For example, the electron density images in Figures 6a,b and 7 are in fair harmony with the atom arrangements in Figures 3a,b and 4a, respectively. We therefore concluded that, as long as the crystal structure was expressed by a structural model, the present split-atom model would be satisfactory.

**(4) Hydration Behavior.** The specific surface areas were  $1.0 \text{ m}^2/\text{g}$  for  $\text{Ca}_7\text{ZrAl}_6\text{O}_{18}$  and  $15.5 \text{ m}^2/\text{g}$  for gypsum. The hydration of  $\text{Ca}_3\text{Al}_2\text{O}_6$  in a previous study<sup>21</sup> was conducted for the powder specimen of comparable fineness and specific surface area. Hence, it is expected that the hydration of the present samples would proceed under similar conditions.

(19) Mondal, P.; Jeffrey, J. W. *Acta Crystallogr., Sect. B* **1975**, *31*, 689–697.

(20) Shannon, R. D. *Acta Crystallogr., Sect. A* **1976**, *32*, 751–767.

(21) Stephan, D.; Wistuba, S. *Cem. Concr. Res.* **2006**, *36*, 2011–2020.

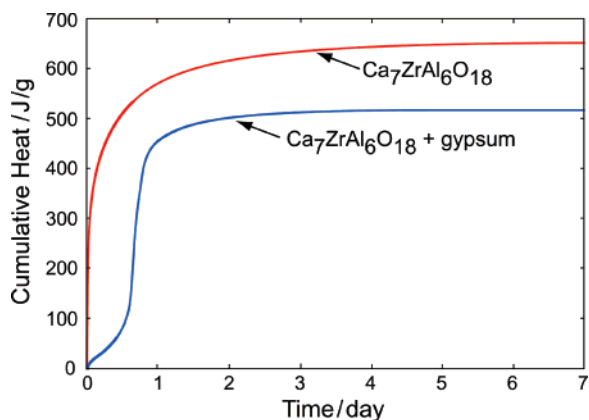


**Figure 8.** Cumulative heat of hydration at 293 K for  $\text{Ca}_7\text{ZrAl}_6\text{O}_{18}$  with and without gypsum.

Without gypsum  $\text{Ca}_7\text{ZrAl}_6\text{O}_{18}$  reacted with water almost immediately after mixing (Figure 8). The hydration reaction was free from premature setting and proceeded gradually for as long as 7 d. This is distinct from the hydration behavior of  $\text{Ca}_3\text{Al}_2\text{O}_6$ , because the reaction normally is almost complete within several hours. The cumulative heat evolution of  $\text{Ca}_7\text{ZrAl}_6\text{O}_{18}$  for 7 d was 652 J/g, which is comparable to that of  $\text{Ca}_3\text{Al}_2\text{O}_6$  for 1 d ( $\sim 750$  J/g).<sup>21</sup> The hydration products of  $\text{Ca}_7\text{ZrAl}_6\text{O}_{18}$  were mainly composed of  $\text{C}_3\text{AH}_6$  with a very small amount of  $\text{C}_4\text{AH}_{19}$ . In the presence of gypsum the reaction experiences a long induction period of  $\sim 12$  h, indicating that the gypsum significantly had the retarding effect on the hydration. The hydration products were

$\text{C}_4\text{A}\bar{\text{S}}\text{H}_{12}$  and  $\text{C}_4\text{AH}_{19}$ . As a result, the hydration products were similar to those for  $\text{Ca}_3\text{Al}_2\text{O}_6$  in both cases with and without the retarder.

$\text{Ca}_3\text{Al}_2\text{O}_6$  constitutes 5–10% of normal Portland cement clinkers. Because the hydration behavior of  $\text{Ca}_7\text{ZrAl}_6\text{O}_{18}$  was comparable to that of  $\text{Ca}_3\text{Al}_2\text{O}_6$  and also free from premature setting, we might be able to develop an advanced substitute, which contains  $\text{Ca}_7\text{ZrAl}_6\text{O}_{18}$  taking the place of  $\text{Ca}_3\text{Al}_2\text{O}_6$ , for the conventional Portland cement.

### Conclusion

The highly disordered crystal structure of  $\text{Ca}_7\text{ZrAl}_6\text{O}_{18}$  was successfully determined from XRPD data. The structure was expressed by the split-atom model, in which the five types of Ca atoms and four types of  $\text{AlO}_4$  tetrahedra were, respectively, positionally and orientationally disordered. The validity of the structural model was verified by the electron density distribution, the structural bias of which was reduced as much as possible using the MPF method. This compound showed the hydration behavior comparable to  $\text{Ca}_3\text{Al}_2\text{O}_6$ .

**Acknowledgment.** Thanks are due to Dr. M. Ichikawa, Taiheiyo Cement Co., for valuable discussion on the hydration reaction.

**Supporting Information Available:** Crystallographic information in CIF format. This material is provided via the Internet at <http://pubs.acs.org>.

CM070731Z